IEEE Photonics Journal
An IEEE Photonics Society Publication

Terahertz Computed Tomography of High-Refractive-Index Objects Based on Refractive Index Matching

Volume 10, Number 6, December 2018

Linyu Chen
Yuye Wang
Degang Xu
Yuchen Ren
Yixin He
Changzhao Li
Chao Zhang
Longhuang Tang
Chao Yan
Jianquan Yao

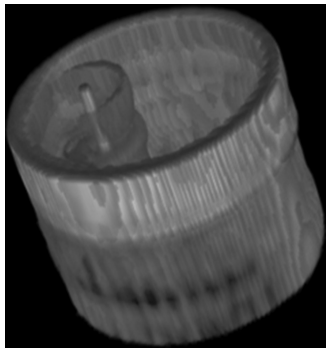

DOI: 10.1109/JPHOT.2018.2877657
1943-0655 © 2018 IEEE

IEEE photonics SOCIETY

IEEE

Terahertz Computed Tomography of High-Refractive-Index Objects Based on Refractive Index Matching

Linyu Chen,[1,2] Yuye Wang,[1,2,3] Degang Xu,[1,2] Yuchen Ren,[1,2] Yixin He,[1,2] Changzhao Li,[1,2] Chao Zhang,[1,2] Longhuang Tang,[1,2] Chao Yan,[1,2] and Jianquan Yao[1,2]

[1]Institute of Laser and Optoelectronics, School of Precision Instruments and Optoelectronics Engineering, Tianjin University, Tianjin 300072, People's Republic of China
[2]Key Laboratory of Optoelectronic Information Science and Technology (Ministry of Education), Tianjin University, Tianjin 300072, People's Republic of China
[3]Department of Neurosurgery and Key Laboratory of Neurotrauma, Southwest Hospital, Third Military Medical University (Army Medical University), Chongqing 400038, People's Republic of China

DOI:10.1109/JPHOT.2018.2877657

Manuscript received September 13, 2018; revised October 19, 2018; accepted October 20, 2018. Date of publication October 23, 2018; date of current version November 7, 2018. This work was supported in part by The National Basic Research Program of China (973) under Grant 2015CB755403 and Grant 2014CB339802, in part by the National Key Research and Development projects under Grant 2016YFC0101001, in part by the National Natural Science Foundation of China under Grant 61775160, Grant 61771332, and Grant 61471257, in part by China Postdoctoral Science Foundation under Grant 2016M602954, and in part by the Postdoctoral Science Foundation of Chongqing under Grant Xm2016021. *(Linyu Chen and Yuye Wang contributed equally to this work.)* Corresponding author: Yuye Wang (e-mail: yuyewang@tju.edu.cn).

Abstract: Terahertz (THz) computed tomography (CT) is a promising technique to obtain the internal information of objects due to its properties of nonionizing and high penetration of nonpolar objects. However, THz CT is hindered by the strong refractive effect and Fresnel reflection loss when it is applied to high-refractive-index samples. In this paper, the three-dimensional image of the sample is performed in the low absorption liquid, the refractive index of which is close to the sample. This novel experimental procedure can eliminate the refractive effect and Fresnel reflection loss effectively. Together with the data processing to eliminate the liquid absorption and to restrain the artifacts, the THz CT imaging of high-density polyethylene ($n = 1.53$) cylinders and cubes is achieved successfully. The internal hole and metallic foreign body are shown accurately. In addition, the defects with different sizes inside the sample are measured with refractive index matching method. It shows that THz CT imaging based on refractive index matching method has high sensitivity to detect the small defect inside the sample as small as 0.5 mm diameter.

Index Terms: Terahertz, computed tomography, high-refractive-index.

1. Introduction

Terahertz (THz) wave spans the frequency ranges from 0.1 THz to 10 THz between the microwave and far infrared regions in the electromagnetic spectrum. It proposes attractive physical characteristics of safety, good penetration depth, and fingerprint spectrum. All these characteristics make THz wave very promising for imaging, which has been proven valuable in numerous fields of medical diagnostics [1], semiconductor wafer examination [2], water content measurement [3], and so

on. Considering that the traditional THz 2D imaging can only provide the whole or the surface information of the object, it is inadequate for the practical application. Recently, much attention has been focused on THz tomography imaging such as THz time-of-flight tomography [4], THz diffraction tomography [5], and especially THz computed tomography (CT) [6]–[10]. THz CT is the extension of X-Ray CT in the electromagnetic spectrum, which is one of the most widely applied 3D imaging techniques based on the concept of Radon transform. Similarly, it makes use of computer-processed combinations of many THz-ray measurements taken from different scanning angles to produce cross-sectional images of an object. The visual representation of the obtained raw data is called a Sinogram. The Sinogram data is processed using a form of tomographic reconstruction, which produces a series of tomographic images, allowing us to see the object inside without cutting [11]. In comparison, X-Ray CT has a limitation to visualize low contrast tissues and structures due to their low absorption. THz wave has good transparency through non-polar materials, and the spatial resolution is suitable for practical imaging applications. In addition, THz wave has the broad spectral bandwidth, making the spectroscopic THz CT possible [12], [13]. Therefore, we could get plenty of information of the sample through THz CT. Since the first report on THz CT in 2002 [6], THz CT has been rapidly developed.

Commonly, the reconstruction algorithm of THz CT originates from X-Ray CT, where the reconstruction algorithm assumes that the diffraction, refractive effect and Fresnel reflection loss can be neglected. This neglect is reasonable because the refractive indices of objects verge on 1 in X-Ray band, which induces no refractive effect and Fresnel reflection loss. However, THz wave shows wave character as well as ray character, the propagation beam is close to a Gaussian distribution. Thus, the diffraction, scattering, Fresnel reflection loss, and especially refractive effect will strongly disturb the image. In the early studies of THz CT, the problem has emerged in the imaging of high-refractive-index samples such as turkey bone and Teflon. The reconstructed image showed the incorrect presence of hole in the center, because the transmitted beam was deviated strongly due to the refractive effect [6], [14]. To date, the majority of works on THz CT focused on imaging of low-refractive-index samples such as polystyrene foam ($n = 1.02$) [15]–[17], thermal protection foam [18] and the samples with hollow structure that seldom suffer from refractive effect [19]–[21]. Although a few researches of THz CT imaging of high-refractive-index objects have been reported [22], they are limited to the imaging of refractive index based on the time delay of THz pulse, which is not as much influenced by refractive effect as attenuation is. However, for the THz CT imaging of absorption coefficient based on the attenuation of intensity, the refractive effect is still problematic. To eliminate the refractive effect in THz imaging, the refractive index matching, as a common method in visible or near-infrared light tomography [23], [24], has been used in THz region. In 2010, K. Kawase *et al.* used a Teflon cover to match the refractive index of sample [25]. However, this method is limited to the cylindrical sample because the profile of the sample with other shapes will change during the rotation. In 2016, their group used the THz lenses with big diameter (63.5 mm) after the sample to make all the refracted beams collected and focused on the detector. This method can suppress the refractive effect to a certain extent [26].

Recently, some researchers considered these effects by modifying the algorithm. E. Abraham *et al.* proposed a multi-peak averaging method to properly determine the time delay of the THz pulse which was severely disturbed by the refractive effect [22]. B. Recur *et al.* developed an improved reconstruction method taking into consideration the physical properties of Gaussian beam to increase the overall quality and accuracy of the reconstructions [27], [28]. S. Mukherjee *et al.* proposed a correction algorithm to compensate for the beam steering as well as Fresnel reflection loss by the simulated theoretical signal with ray tracing software. This method can significantly reduce the boundary effect of cylindrical sample [29]. J. Tepe *et al.* introduced a modified algebraic reconstruction technique (ART) by taking into account the refractive effect according to Snell's law and the Fresnel reflection loss. The reconstruction algorithm used travel time and transmission data simultaneously to reconstruct the refractive index and absorption coefficient of the sample [30]. However, these mathematical methods mentioned above that modify the refractive effect and Fresnel reflection loss are limited to the samples with simple shape. Especially for the imaging of

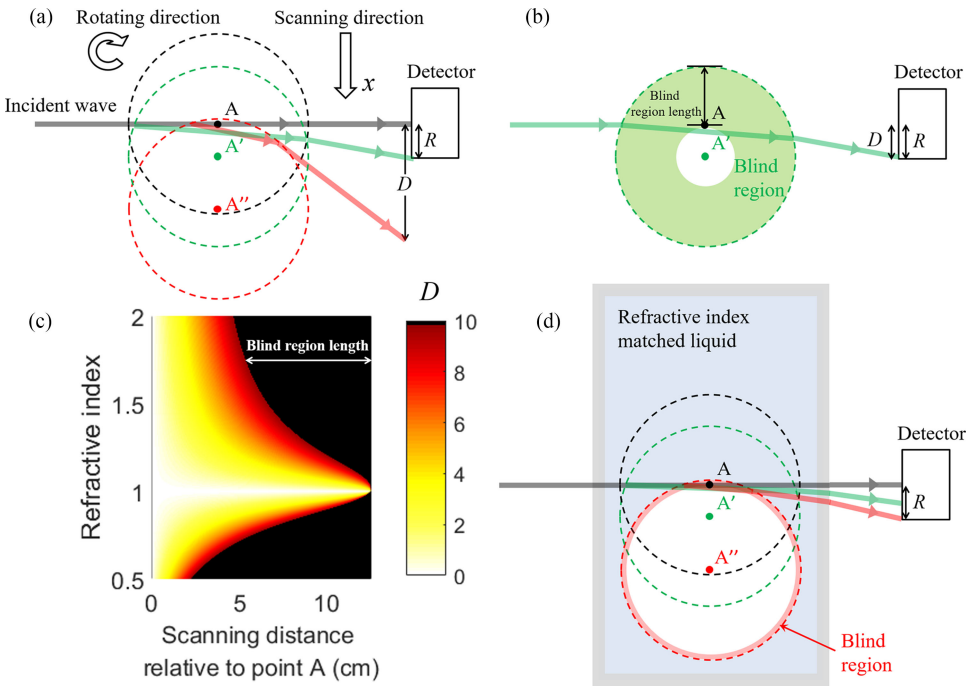

Fig. 1. (a) Beam paths of THz wave with the traditional method in scanning position A, A', and A". (b) Schematic diagram of "blind region". (c) Numerical analysis of beam deviation. (d) Beam path of THz wave with the refractive index matching method.

high-refractive-index samples ($n > 1.3$), the THz beam is deviated strongly, even worse, it cannot be detected. Thus, noises are instead of most image data so that these methods are not suitable.

In this paper, we aim at solving this problem experimentally to prevent the light from deviation in THz CT. A sink filled with refractive index matched liquid is used in our experiment. The sample is immersed in the liquid. During the scanning process of imaging, the liquid sink is fixed perpendicularly to the THz beam. Such method can avoid the refraction and reflection effectively. Moreover, the data processing to eliminate the absorption of liquid and to restrain the artifacts is utilized in the THz CT imaging procedure. The THz CT imaging of cylindrical samples and cuboid samples is successfully realized with the refractive index matching method. Especially, the internal holes with different sizes in cylinders are imaged, where the hole with the 0.5 mm diameter is clearly displayed in the reconstructed image. The results indicate that THz CT imaging has high sensitivity to detect the small defect inside the sample.

2. Method

2.1 Refractive Effect and FRESNEL Reflection Loss Elimination Based on Refractive Index Matching

Refractive effect is the main problem that has to be solved in THz CT. We put the sample in a sink filled with refractive index matched liquid to overcome the problem. Here, we take a cylindrical sample as an example to prove the feasibility of refractive index matching method theoretically. Figs. 1(a) and 1(b) show the light paths of THz beam with the traditional method, where THz beam directly incidents into the sample, and it is focused on the sample center. The three points A, A', and A" represent three scanning positions along the scanning direction. When the sample center moves to the three scanning positions, the sample is represented as black, green and red dashed circles respectively. Correspondingly, the light paths are marked by the lines with the same color.

We assume that the refractive index of the sample is 1.53, the diameter of the sample is 25 mm, the radius R of the detector is 10 mm, the physical distance between the detector and the focal spot of THz beam is 25 mm, and the beam diameter of THz wave is neglected for simplicity. D represents the deviation of THz beam compared with the detector center along the detector plane. As we can see from Fig. 1(a), when the sample center is in position A, the THz beam is perpendicular to the sample, and there is no deviation on the detector plane. When the sample center is in position A', the beam deviation is equal to R, which represents the critical situation. Furthermore, when the center of sample is in position A", the beam deviation is larger than R, and the light cannot be detected in this case.

It can be seen that, along the scanning direction from A to A", the light can be only detected between the scanning position of A and A'. Therefore, the scanning region of sample in other scanning position is called the blind region [29]. Considering the rotation of sample during CT imaging, the blind region of the sample should be a circular ring. As shown in Fig. 1(b), the green part represents the blind region of the sample. For simplicity, the "blind region length", defined as the scanning distance with no light detected, is used here to measure the size of blind region. From Fig. 1(b), it is clearly seen that the blind region almost occupies the whole sample, which will definitively influence the imaging result. We calculate the theoretical deviation D of the light on the detector plane, as shown in Fig. 1(c). The x, y, and z axes of the image represent the scanning distance relative to point A, the refractive index of sample and the deviation, respectively. The black area corresponds to the deviation value greater than R (10 mm) where the light is not detected, and the transverse length of black area represents the blind region length. It is seen that when the relative refractive index is larger than 1.10, the blind region will affect the image result. When the relative refractive index is between 0.95 to 1.10, the blind region length can be negligible.

The refractive index matching method can reduce the relative refractive index of sample by immersing the sample in a sink filled with refractive index matched liquid. We take the liquid with refractive index of 1.46 as an example. When the sample is immersed and scanned in the liquid, the relative refractive index of sample is calculated as $1.53/1.46 = 1.05$. As shown in Fig. 1(d), the incident light is not refracted on the interface of liquid sink because the front surface of liquid sink is perpendicular to the THz beam. On the interface between liquid and sample, the THz beam is just slightly deviated because the relative refractive index of sample is close to 1. In consequence, along the scanning position from A to A", the deviation of THz beams is strongly reduced compared with the traditional method. The light can be detected even when the sample center is in position A". This certifies that the refractive index matching method can effectively eliminate the refractive effect. Although the blind region (red area) still exists, it is much smaller. Therefore, the THz CT imaging of high-refractive-index sample can be realized.

2.2 Elimination of Liquid Absorption

When the sample is scanned in liquid, the shape of liquid is changing all the time. Considering the lack of low-absorption liquid in THz band, the absorption of liquid will affect the results. To reduce the effect of liquid, we need a priori information on the shape of sample and the absorption coefficient of liquid. Thus, the transmittance of liquid can be eliminated simply through dividing the measured raw transmittance data by the simulated transmittance of liquid. The flowchart in Fig. 2 demonstrates the data processing to eliminate the noise of liquid. A cubic sample with a higher absorption part in the lower right is taken as an example. The coordinate of the investigated point is represented as (i, j), and the absorption coefficient of the sample is represented as the matrix of $f(i, j)$. The raw transmittance Sinogram data including the noise of liquid is expressed as follows according to Lambert-Beer Law,

$$T_0(\theta, \rho) = \frac{1}{\exp\{Radon[f(i, j)]\}} \cdot T_{liq}(\theta, \rho) \tag{1}$$

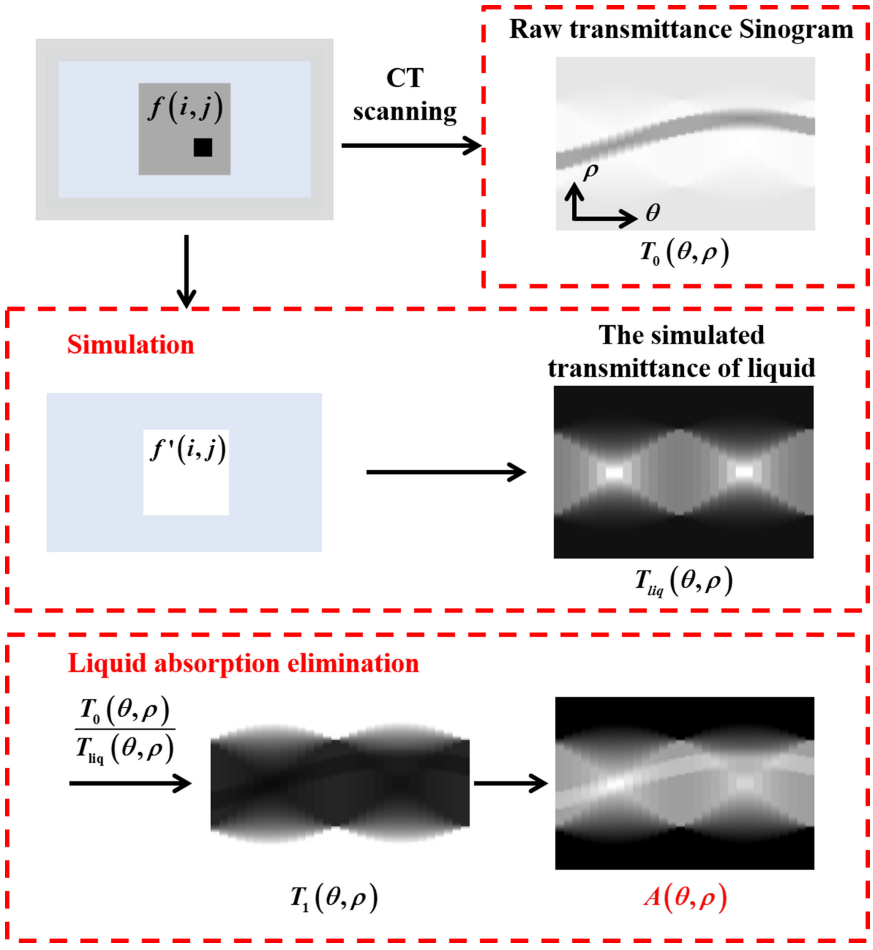

Fig. 2. Flowchart of the liquid absorption elimination approach.

Here, $T_{liq}(\theta, \rho)$ is the transmittance of liquid, and the Radon function represents the Radon transform as

$$Radon\left[f\left(i,j\right)\right] = \int_{-\infty}^{\infty}\int_{-\infty}^{\infty} f\left(i,j\right)\delta\left(\rho - i\cos\theta - j\sin\theta\right)didj \tag{2}$$

where δ is the Dirac impulse, θ and ρ are the projection angle and position respectively. If the shape information of the sample is available beforehand, a simulated matrix $f'(i, j)$ can be constructed. Then, the transmittance of liquid can be simulated as

$$T_{liq}\left(\theta,\rho\right) = \exp\left\{Radon\left[f'\left(i,j\right)\right]\right\} \tag{3}$$

Thus, the noise of liquid can be eliminated by

$$T_1\left(\theta,\rho\right) = T_0\left(\theta,\rho\right)/T_{liq}\left(\theta,\rho\right) \tag{4}$$

and the absorption Sinogram can be given by

$$A\left(\theta,\rho\right) = \ln\left(1/T_1\left(\theta,\rho\right)\right) \tag{5}$$

It should be mentioned that, the procedure in this Section could be ignored if the absorption of liquid is much lower than that of the sample.

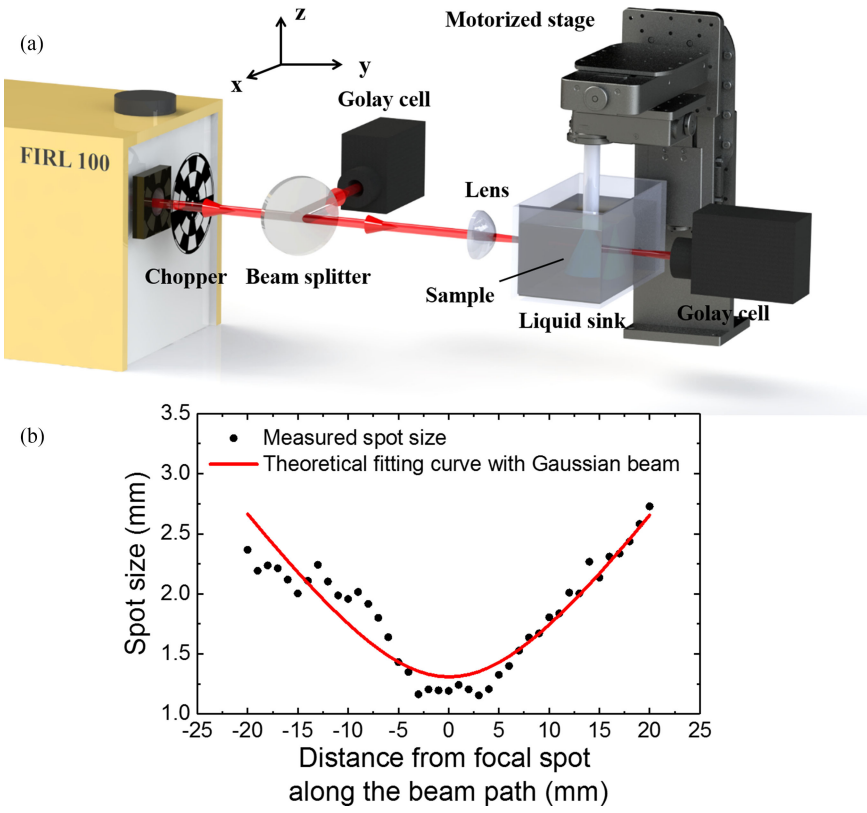

Fig. 3. (a) The experimental setup of THz CT imaging system based on refractive index matching. (b) Spot size measurements along the beam path.

2.3 Preprocessing Before Reconstruction Algorithm

As stated in Section 2.1, although the refractive index matching method can eliminate the refractive effect effectively, the blind region still exists. When the light is not detected due to the deviation, the measured intensity of the transmitted light is near zero. Thus, the corresponded absorption coefficient in the Sinogram is abnormally high. As a result, there are numerous artifacts in the reconstructed image. Similar problem also exists in X-Ray CT, called as metal artifact [31]. Many methods have been proposed to reduce the metal artifacts in X-Ray CT, but they are not suitable for THz CT because the blind region is more complicated. In this paper, we refer to the nonlinear weights method proposed by J. Gu *et al.* [32], and a simple function is used here to depress the abnormally high value by making use of the logarithmic function as follows,

$$A'(\theta,\rho)=\begin{cases}\log_{10}\left(A(\theta,\rho)-t+1\right)+t, & A(\theta,\rho)>t\\ A(\theta,\rho), & A(\theta,\rho)\le t\end{cases} \tag{6}$$

where $A'(\theta,\rho)$ is the processed Sinogram data, and t is the threshold of the abnormally high value. Based on Eq. (6), the normal data will not be changed, whereas the abnormally high data (higher than the threshold) will be strongly restrained. After this simple process, the artifacts can be reduced and the contrast between the sample and background can be improved. The relative error for the abnormal data is not considered here.

3. Experimental Setup

The THz CT imaging system is schematically shown in Fig. 3(a). A tunable continuous THz gas laser (FIRL100, Edinburgh Instruments Ltd.) operating at 2.52 THz is used in the imaging system

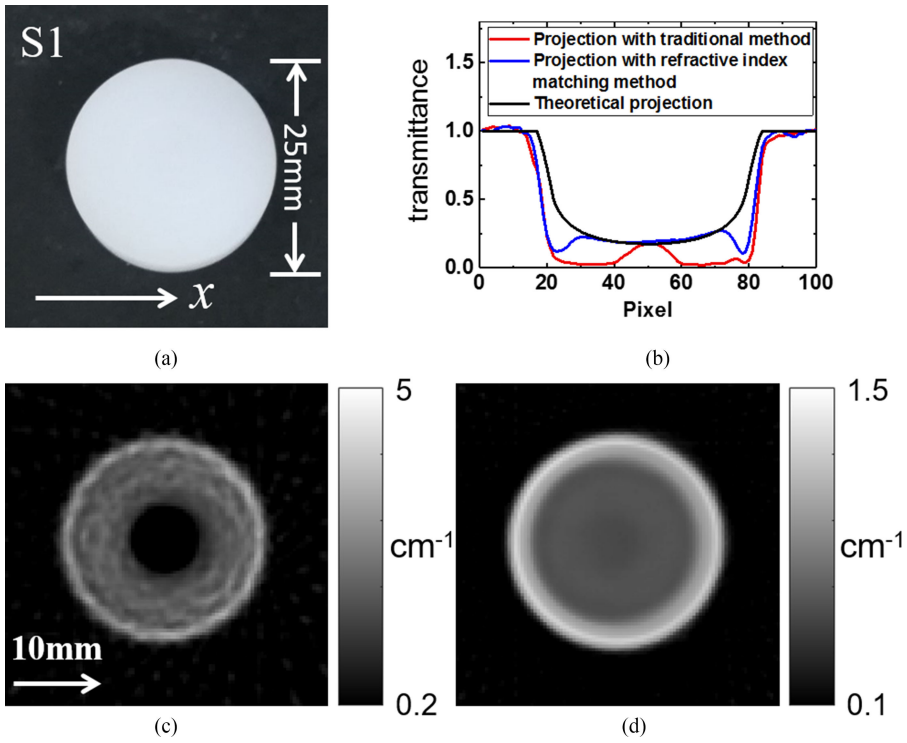

Fig. 4. (a) Photograph of the HDPE cylindrical Sample 1. (b) Projections of the sample in one scanning angle. (c) The reconstructed image with the traditional method. (d) The reconstructed image with the refractive index matching method.

for its high average output power up to 150 mW. Two Golay cells (GC-1P, Tydex Ltd) are used to measure the intensity of THz wave. Owning to the responsivity of the Golay cell, a chopper operating at 50 Hz is used to modulate the THz wave. In order to remove the noise from slight power fluctuations, the THz wave is separated by a wire-grid beam splitter into a reference beam and a signal beam. The signal beam is focused on the sample center by using a Tsurupica lens ($f = 50$ mm). A rectangular liquid sink made of high-density polyethylene (HDPE) is placed on a fixed place. The front and back surface of the sink is perpendicular to the beam. The sample is mounted on a computer controlled rotation motorized stage that rotates around the z axis. And the rotation motorized stage is mounted on a computer controlled x-z linear motorized stage. The sample is immersed and scanned inside the sink which is filled with the refractive index matched liquid. The THz beam transmitted through the sample is collected by the Golay cell directly, in order to reduce the light path as much as possible. The distribution of spot size ranges from -20 mm to 20 mm along the beam path is measured through knife-edge method, as shown in Fig. 3(b). The focal spot size is about 1.1 mm, and the Rayleigh length is estimated to 11.2 mm from the theoretical fitting curve with Gaussian beam, which is plotted as the red line in Fig. 3(b).

4. Results and Discussion

4.1 Cylindrical Sample

The THz CT imaging based on the refractive index matching method is firstly performed on a cylindrical (25 mm in diameter) HDPE sample, as shown in Fig. 4(a). The liquid paraffin is chosen to be the refractive index matched liquid. The refractive index of the liquid paraffin and HDPE are measured to be 1.46 and 1.53 respectively at 2.52 THz with a time-domain spectroscopy (TDS) system (TAS7500TS, Advantest Co.). The sample is scanned from -20 mm to 20 mm along x axis

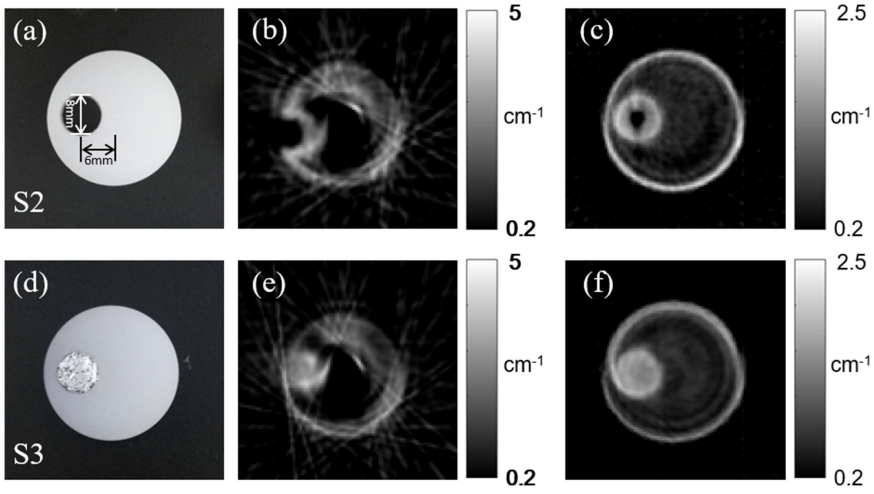

Fig. 5. (a) Photograph of the Sample 2. The reconstructed images of Sample 2 with (b) the traditional method and (c) the refractive index matching method. (d) Photograph of the Sample 3. The reconstructed images of Sample 3 with (e) the traditional method and (f) the refractive index matching method.

with a scanning step of 400 μm. After each line-scanning, the sample rotates with a certain angle, and the rotation step is 6°, corresponding to the projection number of 30. It took about 5 minutes to obtain a tomographic 2D image with 100 $\times$ 100 pixels. Here, the filtered back projection (FBP) algorithm, which is the most widely used algorithm in many CT device, is utilized to reconstruct the image from the Sinogram obtained with the traditional method and the refractive index matching method, respectively. And the FBP algorithm is performed on MATLAB software. Fig. 4(b) gives the cross-sectional projections of the sample in one scanning angle. The red line represents the projection with the traditional method (i.e., scanned in the air). Compared with the theoretical projection (black line) calculated according to Lambert-Beer Law, it is seen that most transmittance values in red line between -12.5 mm to 12.5 mm are very close to zero because the transmitted beam is not detected. As a result, there is an erroneous hole in the central area of the cross-sectional reconstructed image with the traditional method, as shown in Fig. 4(c). Here, the white color indicates the high absorption coefficients whereas the black color indicates the low absorption coefficients of the THz wave. The estimated absorption coefficients are unreasonable in the central dark hole of the image, where the values are negative. And the mean value in sample region is about 1.57 cm^{-1}, which is bigger than the actual absorption coefficient (0.68 cm^{-1}) of the HDPE sample we used. From the projection with the refractive index matching method, marked as a blue line in Fig. 4(b), it is clear that the measured transmittance is approximate to the theoretical projection. Thus, the reconstructed image with the refractive index matching method is more accurate and homogeneous, as shown in Fig. 4(d). The mean value in sample region (0.53 cm^{-1}) is much closer to the actual value. Notice that there is a bright ring in the boundary of the sample, this phenomenon is called as "edge effect" [33]. It's mainly attribute to that the refractive index of liquid cannot be perfectly matched with that of the sample. In other words, the small area near the boundary is still the blind region. This result is in good agreement with the theoretical analysis in Section 2.1.

To demonstrate the ability of THz CT imaging to detect the internal defect and foreign body, another two samples are tested. Sample 2 is a HDPE cylinder (25 mm in diameter) drilled with an off-axis hole (8 mm in diameter) which is 6 mm deviated from the sample center, as shown in Fig. 5(a). Fig. 5(b) gives the cross-sectional reconstructed imaging result with the traditional method. It is seen that although the outer profile of the sample is reconstructed, the internal hole can't be identified. In comparison, the imaging result with the refractive index matching method is much better, as indicated in Fig. 5(c). The internal hole is shown clearly and the artifacts are obviously reduced. However, it is noted that the reconstructed hole in Fig. 5(c) appears like a bright

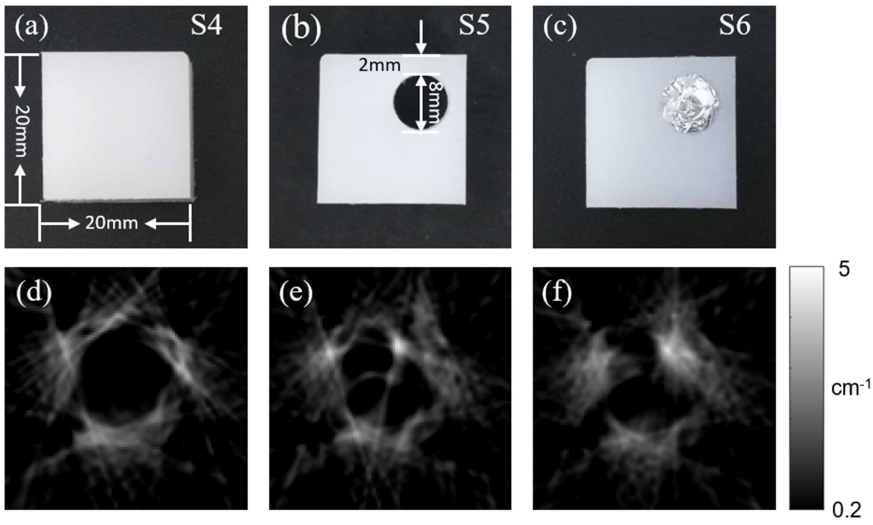

Fig. 6. Photographs of the HDPE cuboid (a) Sample 4, (b) Sample 5 and (c) Sample 6. Reconstructed images of (d) Sample 4, (e) Sample 5 and (f) Sample 6 with the traditional method.

circle with a dark area in the center, where the pixel values in some regions are much higher than that in the air region, although the hole in theoretical image should be an entire dark circle due to the fact that the absorption coefficient value of air is zero. This is caused by the edge effect of the hole. Considering that the refractive index matching method can't be applied to the internal hole, there is no effective solution for this problem currently. Then, we put some metallic foreign body in the hole as Sample 3, as shown in Fig. 5(d). Fig. 5(e) gives the reconstructed image of Sample 3 with the traditional method. The foreign body is shown faintly, but the internal structure is inaccurate and the image is strongly distorted by artifacts. In contrast, the shape and position of foreign body can be seen clearly in the reconstructed image with the refractive index matching method, as shown in Fig. 5(f).

4.2 Cuboid Sample

In the practical application, the object usually has different shape. The incident and exit angles on the interface change with not only scanning position but also scanning angle. The refractive effect is much more complicated and unpredictable. In this section, we apply the refractive index matching method on three cuboid samples with the cross section size of 20 mm $\times$ 20 mm, as shown in Figs. 6(a)–6(c). Sample 4 is a HDPE cube. Sample 5 is a HDPE cube with an internal hole of 8 mm diameter, and Sample 6 is a HDPE cube with a cylindrical foreign body inside. Figs. 6(d)–6(f) are the reconstructed images of the samples with the traditional method, which are strongly distorted by noise, and cannot show any information, even the profile of the sample. These results illustrate that the refractive effect severely affects the reconstructed THz CT image of high-refractive-index non-cylindrical sample, making it difficult to be distinguished.

Then, the samples are imaged with the refractive index matching method. Figs. 7(a) and 7(e) are the theoretical Sinogram of Sample 4 and the corresponding reconstructed image, which are used for comparison. Figs. 7(b)–7(d) show the Sinogram of absorption coefficient for Sample 4, Sample 5 and Sample 6 with the refractive index matching method, respectively. Correspondingly, the reconstructed images are presented in Figs. 7(f)–7(h), respectively. It is obvious that the reconstructed profiles of Sample 4, Sample 5 and Sample 6 are very close to the theoretical simulation and the real objects. The spatial identification of the internal hole and foreign body is clearer and the image quality of the measured slice can be much improved. This result confirms that THz CT based on the refractive index matching method can reduce the refractive effect effectively to some

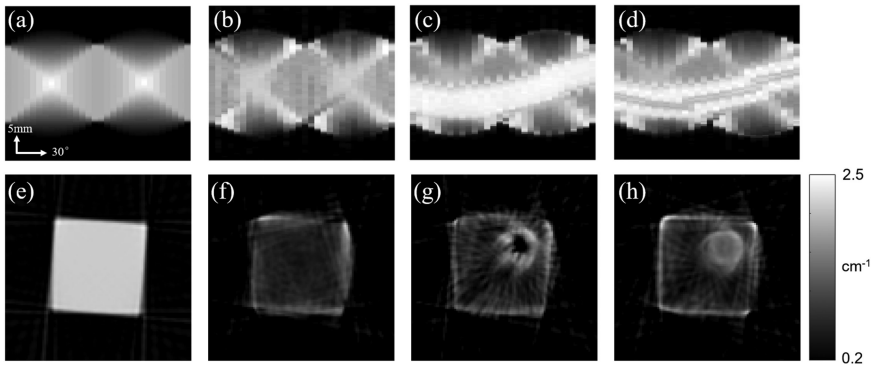

Fig. 7. (a) Theoretical Sinogram of Sample 4. Actual Sinogram of (b) Sample 4, (c) Sample 5 and (d) Sample 6 with the refractive index matching method. (e) Theoretically reconstructed image of Sample 4. Reconstructed image of (f) Sample 4, (g) Sample 5 and (h) Sample 6 with the refractive index matching method.

extent. Compared with Fig. 7(e), the reconstructions in Figs. 7(f)–7(h) still suffer from some artifacts. One reason is the limited projection number, which influences the 3D tomographic reconstruction using FBP algorithm. Theoretically, an ideal image can be achieved with THz CT, provided that the data are sampled at enough projection angles that a fine enough reconstruction grid is ensured. When the projection number is 30, there are a few artifacts in existence even in Fig. 7(e). Therefore, the image quality can be improved through increasing the projection number at the cost of time. Another reason is that the refractive effect cannot be completely eliminated using the liquid paraffin due to the refractive index mismatch, as explained previously, inducing the abnormal high values in the Sinogram and furtherly resulting in the artifacts in the reconstruction, which can be obviously observed through comparing Figs. 7(b)–7(d) with Fig. 7(a), respectively. Thus, the better refractive index matched liquid medium is still in great demand to achieve the weaker index mismatch. Additionally, the accuracy of this method is also influenced by the algorithm to depress the abnormally high value, which depends on the better mathematical improvements to the algorithm. Finally, the complexity of sample shape is an important factor influencing the accuracy as well, because the liquid absorption elimination is hard to be performed precisely in such a case.

4.3 The Discernibility of THz CT

As we discussed in Section 4.1, the hole inside the sample cannot be well reconstructed as an ideal dark region due to the edge effect of itself. This indicates that the edge effect may affect the distinguishable ability of the presence of internal contents for THz CT. In this section, the cylindrical HDPE samples (25 mm in diameter) with internal holes of different diameters (5 mm, 3 mm, 1 mm, and 0.5 mm), as shown in Figs. 8(a)–8(d), are imaged to analyze the discernibility of THz CT with the refractive index matching method. Figs. 8(e)–8(h) give the imaging results of the samples. The cross-sectional reconstructed images of holes with diameters of 5 mm and 3 mm in cylinders are shown as a bright circle with a dark hole, similar to the imaging result of Sample 2. However, when the diameters of the holes are 1 mm and 0.5 mm, the holes in corresponding reconstructions are displayed as the entire bright circles, which are almost same with the imaging results for the hole filled with metallic foreign body. Considering the wavelength λ of THz wave is about 119 μm in our experiment, these facts indicate that the THz CT cannot determine the internal contents when the internal hole size is smaller than 10λ. Figs. 8(i)–8(l) give the profiles of these images along the red lines crossed the defect centers shown in Figs. 8(e)–8(h), by plotting the pixel values of absorption coefficient as a function of the position. If we take the position of peak value as the boundary of sample and hole, the size of the samples is measured to be 24.4 mm, which is close to the actual sample size of 25 mm. The sizes of the holes in Figs. 8(i) and 8(j) are estimated to be 4.0 mm

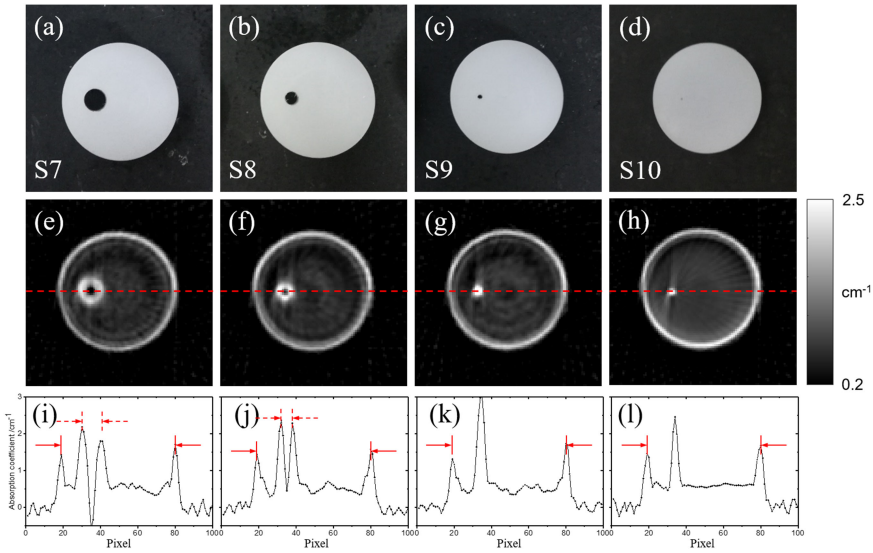

Fig. 8. Photographs of (a) Sample 7, (b) Sample 8, (c) Sample 9 and (d) Sample 10. Reconstructed images of (e) Sample 7, (f) Sample 8, (g) Sample 9 and (h) Sample 10 with the refractive index matching method. Absorption coefficients distribution along the dashed lines of (i) Sample 7, (j) Sample 8, (k) Sample 9 and (l) Sample 10.

and 2.4 mm, respectively. There is only one peak generated in Figs. 8(k) and 8(l) due to the small hole, so the hole sizes are not given. The measured absorption coefficients in air regions should be almost zero, but those in the hole regions take finite values as shown in Figs. 8(i) and 8(j). This is attribute to the poor spatial resolution. If the beam diameter is sufficiently less than the hole diameter, the error can be reduced.

Although the THz CT based on refractive index matching method enable neither edge-effect-free reconstruction nor quantitative measurement for the internal structure, it shows excellent ability to distinguish defect inside the sample. As we can see in Fig. 8(d), the hole with a diameter of 0.5 mm in the photograph is very dim. However, the corresponding hole in the reconstructed image of THz CT emerges very conspicuous, thanks to the edge effect of the internal defect. This result illustrates that the THz CT imaging is sensitive to the small defect inside the sample which is much smaller than the spot size, and it can evaluate the internal structure of objects qualitatively. It is obviously useful in the practical regions, like non-destructive testing and art conservation.

Finally, in order to highlight the potential application of THz CT imaging, we demonstrate the 3D THz CT imaging based on refractive index matching method on a cylindrical HDPE sample (30 mm in diameter) with an internal hole (10 mm in diameter) which is 8 mm deviated from the center. The internal hole is divided into three equal parts, where the part A is empty, and the part B and part C are filled with metallic foreign body and paraffin wax, respectively. Especially, a needle is vertically inserted in the center of part C to make the sample complex, as shown in Fig. 9(a). The sample with a total thickness of 24 mm is split into 12 slices spaced by 2 mm. The tomographic 2D imaging of 12 slices is executed with the above-mentioned experimental procedure. Then, the 3D reconstruction of the sample is performed from 12 tomographic 2D images using the ImageJ software.

Figures 9(b) and 9(c) show the 3D reconstruction in different viewing angle. Here, it is noted that the homogeneous parts of HDPE and paraffin wax are set to be transparent in the 3D reconstruction, in order to reveal the internal structure. The boundary of paraffin wax and the hidden part of the needle in part C, which are not visible in Fig. 9(a), can be clearly seen in the 3D reconstruction. An animated view of the 3D reconstruction is provided in Visualization 1. Part A and part C can be displayed clearly in the video, whereas part B is not easy to be observed because it is blocked by the outline of sample. Fig. 9(d) gives another representation of 3D reconstruction which offers the

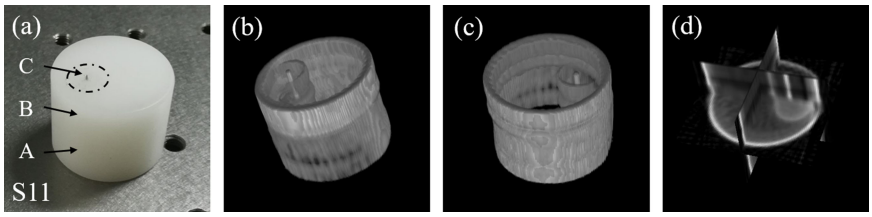

Fig. 9. (a) Photograph of the sample. (b) and (c) 3D reconstruction of the sample in different viewing angle (see Visualization 1). (d) Orthoslices with axial, coronal and sagittal views.

orthoslices with axial, coronreal and sagittal views, allowing us to see the details of internal structure of the sample. From Fig. 9(d), the foreign body in part B can be well displayed. This example of 3D reconstruction of complex object emphasizes the potential of THz CT imaging based on refractive index matching method which provides high quality 3D spatial distribution of samples.

5. Conclusions

In conclusion, we developed a THz CT imaging method based on refractive index matching, to solve the refractive effect and Fresnel reflection loss problem for high-refractive-index objects experimentally. Along with an algorithm to eliminate the absorption of the liquid and to restrain the artifacts, the refractive index matching method is applied to the cylindrical HDPE samples and cuboid HDPE samples, respectively. The quality of the reconstructed images is significantly improved, compared with the imaging results with the traditional method. Moreover, defects with different sizes inside the samples are analyzed with the refractive index matching method. It shows THz CT imaging has high sensitivity to detect the small defect inside the sample as small as 0.5 mm diameter. It is suggested that THz CT imaging based on the refractive index matching method opens an avenue to break through the restriction of traditional THz CT, and extends the potential of THz CT imaging technique to a wider range of application.

References

[1] Y. B. Ji *et al.*, "Terahertz reflectometry imaging for low and high grade gliomas," *Sci. Rep.*, vol. 6, 2016, Art. no. 36040.
[2] S. Ohno, A. Hamano, K. Miyamoto, C. Suzuki, and H. Ito, "Surface mapping of carrier density in a GaN wafer using a frequency-agile THz source," *J. Euro. Opt. Soc. Rap. Publ.*, vol. 4, 2009, Art. no. 09012.
[3] Y. Wang, H. Minamide, M. Tang, T. Notake, S. Lee, and H. Ito, "Study of water concentration measurement in thin tissues with terahertz-wave parametric source," *Opt. Exp.*, vol. 18, no. 15, pp. 15504–15512, 2010.
[4] D. M. Mittleman, S. Hunsche, L. Boivin, and M. C. Nuss, "T-ray tomography," *Opt. Lett.*, vol. 22, no. 12, pp. 904–906, 1997.
[5] S. Wang and X-C. Zhang, "Pulsed terahertz tomography," *J. Phys. D, Appl. Phys.*, vol. 37, no. 4, pp. R1–R36, 2004.
[6] B. Ferguson, S. Wang, D. Gray, D. Abbot, and X.-C. Zhang, "T-ray computed tomography," *Opt. Lett.*, vol. 27, no. 15, pp. 1312–1314, 2002.
[7] J. P. Caumes *et al.*, "Terahertz tomographic imaging of XVIIIth Dynasty Egyptian sealed pottery," *Appl. Opt.*, vol. 50, no. 20, pp. 3604–3608, 2011.
[8] H. Bessou *et al.*, "Three-dimensional terahertz computed tomography of human bones," *Appl. Opt.*, vol. 51, no. 28, pp. 6738–6744, 2012.
[9] S. Mukherjee and J. Federici, "Study of structural defects inside natural cork by pulsed terahertz tomography," in *Proc. Int. Conf. Infrared, Millim. THz Waves*, 2011, pp. 1–2.
[10] H. Balacey, B. Recur, J. B. Perraud, J. B. Sleiman, J. P. Guillet, and P. Mounaix, "Advanced processing sequence for 3-D THz imaging," *IEEE Trans. THz Sci. Technol.*, vol. 6, no. 2, pp. 191–198, 2016.
[11] G. T. Herman, *Fundamentals of Computerized Tomography: Image Reconstruction from Projection*, 2nd ed. New York, NY, USA: Springer, 2009.
[12] A. Brahm, M. Kunz, S. Riehemann, G. Notni, and A. Tunnermann, "Volumetric spectral analysis of materials using terahertz-tomography techniques," *Appl. Phy. B*, vol. 100, no. 1, pp. 151–158, 2010.
[13] E. Kato, S. Nishina, A. Irisawa, T. Yamashita, M. Imamura, and K. Kawase, "3D spectroscopic computed tomography imaging using terahertz waves," in *Proc. IEEE Int. Conf. Infrared, Millim., THz Waves*. 2010, pp. 1–2.
[14] K. L. Nguyen, M. L. Johns, and L. F. Gladden, "Three dimensional imaging with a terahertz quantum cascade laser," *Opt. Exp.*, vol. 14, no. 6, pp. 2123–2129, 2006.

[15] X. X. Yin, B. W.-H. Ng, D. Abbott, J. A. Zeitler, K. L. Nguyen, and L. Gladden, "Local reconstruction for three dimensional terahertz imaging using a CW quantum cascade laser," in *Proc. Int. Conf. Image Process., Comput. Vis. Pattern Recognit.*, 2008 pp. 252–258.
[16] Q. Li, Y-D. Li, S-H. Ding, and Q. Wang, "Terahertz computed tomography using a continuous-wave gas laser," *J. Infrared Millim. THz Waves*, vol. 33, no. 5, pp. 548–558, 2012.
[17] M. Suga, Y. Sasaki, T. Sasahara, T. Yuasa, and C. Otani, "THz phase-contrast computed tomography based on Mach-Zehnder interferometer using continuous wave source: proof of the concept," *Opt. Exp.*, vol. 21, no. 21, pp. 25389–25402, 2013.
[18] D. J. Roth, S. Reyes-Rodriguez, D. A. Zimdars, R. W. Rauser, and W. W. Ussery, "Terahertz computed tomography of NASA thermal protection system materials," *AIP Conf. Proc.*, vol. 1430, pp. 566–572, 2012.
[19] T. Zhou, R. Zhang, C., Yao, Z.-L. Fu, D.-X. Shao, and J.-C. Cao, "Terahertz three-dimensional imaging based on computed tomography with photonics-based noise source," *Chin. Phys. Lett.*, vol. 34, no. 8, pp. 76–78, 2017.
[20] P. Hillger, A. Schluter, R. Jain, S. Malz, J. Grzyb, and U. Pfeiffer, "Low-Cost 0.5 THz computed tomography based on silicon components," in *Proc. Int. Conf. Infrared, Millim., THz Waves*, 2017, pp. 1–2.
[21] M. Jewariya *et al.*, "Fast three-dimensional terahertz computed tomography using real-time line projection of intense terahertz pulse," *Opt. Exp.*, vol. 21, no. 2, pp. 2423–2433, 2013.
[22] E. Abraham, A. Younus, C. Aguerre, P. Desbarats, and P. Mounaix, "Refraction losses in terahertz computed tomography," *Opt. Commun.*, vol. 283, no. 10, pp. 2050–2055, 2010.
[23] S. Meissner, L. Knels, and E. Koch, "Improved three-dimensional Fourier domain optical coherence tomography by index matching in alveolar structures," *J. Biomed. Opt*, vol. 14, no. 6, 2009, Art. no. 064037.
[24] M. Brezinski, K. Saunders, C. Jesser, X. Li, and J. Fujimoto, "Index matching to improve optical coherence tomography imaging through blood," *Circulation*, vol. 103, no. 15, pp. 1999–2003, 2001.
[25] K. Kawase, T. Shibuya, S. Hayashi, and K. Suizu, "THz imaging techniques for nondestructive inspections," *Comptes Rendus Physique*, vol. 11, pp. 510–518, 2010.
[26] S. R. Tripathi, Y. Sugiyama, K. Murate, K. Imayama, and K. Kawase, "Terahertz wave three-dimensional computed tomography based on injection-seeded terahertz wave parametric emitter and detector," *Opt. Exp.*, vol. 24, no. 6, pp. 6433–6440, 2016.
[27] B. Recur *et al.*, "Investigation on reconstruction methods applied to 3D terahertz computed tomography," *Opt. Exp.*, vol. 19, no. 6, pp. 5105–5117, 2011.
[28] B. Recur *et al.*, "Propagation beam consideration for 3D THz computed tomography," *Opt. Exp.*, vol. 20, no. 5, pp. 5817–5829, 2012.
[29] S. Mukherjee, J. Federici, P. Lopes, and M. Cabral, "Elimination of fresnel reflection boundary effects and beam steering in pulsed terahertz computed tomography," *J. Infrared Millim. THz Waves*, vol. 34, no. 9, pp. 539–555, 2013.
[30] J. Tepe, T. Schuster, and B. Littau, "A modified algebraic reconstruction technique taking refraction into account with an application in terahertz tomography," *Inverse Probl. Sci. Eng.*, vol. 25, no. 10, pp. 1448–1478, 2016.
[31] F. E. Boas and D. Fleischmann, "CT artifacts: Causes and reduction techniques," *Imaging Med.*, vol. 4, no. 2, pp. 229–240, 2012.
[32] J. Gu, L. Zhang, Z. Chen, and Y. Xing, "Projection-based metal artifacts reduction in CT images via nonlinear weights," *J. Tsinghua Univ. (Sci. Technol.)*, vol. 46, no. 6, pp. 825–828, 2006.
[33] A. Brahm, A. Wilms, M. Tymoshchuk, C. Grossmann, G. Notni, and A. Tunnermann, "Optical effects at projection measurements for terahertz tomography," *Opt. Laser Technol.*, vol. 62, no. 62, pp. 49–57, 2014.